

# A Proposal for A1/MAMI: Polarization Transfer Measurements in $^{40}\text{Ca}(\vec{e}, e'\vec{p})^{39}\text{K}$ Scattering

P. Achenbach<sup>1</sup>, D. Bosnar<sup>2</sup>, T. Brecej<sup>3</sup>, A. Denig<sup>1</sup>, M.O. Distler<sup>1</sup>, A. Esser<sup>1</sup>, H. Fonvielle<sup>4</sup>, P. Herrmann<sup>1</sup>, M. Hoek<sup>1</sup>, P. Klag<sup>1</sup>, T. Kolar<sup>3</sup>, I. Korover<sup>5,6</sup>, J. Lichtenstadt<sup>5</sup>, I. Mardor<sup>5,7</sup>, H. Merkel<sup>1</sup>, M. Mihovilovic<sup>3</sup>, **U. Müller** (Spokesperson)<sup>1</sup>, J. Müller<sup>1</sup>, **S. Paul** (Spokesperson)<sup>5</sup>, E. Piasezky<sup>5</sup>, J. Pochodzalla<sup>1</sup>, G. Ron<sup>8</sup>, B.S. Schlimme<sup>1</sup>, C. Sfienti<sup>1</sup>, S. Sirca<sup>3</sup>, R. Spreckels<sup>1</sup>, M. Thiel<sup>1</sup>, and I. Yaron<sup>5</sup>

<sup>1</sup>Institut für Kernphysik, Johannes Gutenberg-Universität, Mainz, Germany

<sup>2</sup>University of Zagreb, Zagreb, Croatia

<sup>3</sup>University of Ljubljana, Slovenia

<sup>4</sup>Laboratoire de Physique de Clermont - IN2P3/CNRS Université Clermont Auvergne, France

<sup>5</sup>Tel Aviv University, Tel Aviv, Israel

<sup>6</sup>Nuclear Research Center-Negev, Beer-Sheva, Israel

<sup>7</sup>Soreq Nuclear Research Center, Yavne, Israel

<sup>8</sup>Hebrew University of Jerusalem, Jerusalem, Israel

November 4, 2018

## 1 Introduction

Historically, polarization transfer measurements in elastic  $\vec{e}p \rightarrow e'\vec{p}'$  scattering have been used to measure the ratio of the electric and magnetic elastic form factors (FFs) of the proton,  $G_E$  and  $G_M$ , since the ratio of the transferred polarization components,  $P_x/P_z$ , is related to the ratio of the form factors [1]:

$$\left(\frac{P_x}{P_z}\right)_H = -\frac{2M_p}{(E + E') \tan \frac{\theta}{2}} \frac{G_E^p(Q^2)}{G_M^p(Q^2)} \quad (1)$$

Similar measurements have been performed in *quasielastic* scattering experiments in an effort to determine if the proton FFs are modified inside of a nucleus and reveal a deviation

in the ratio  $P_x/P_z$  when compared to elastic scattering. The double ratio  $\frac{(P_x/P_z)_A}{(P_x/P_z)_H}$  taken between a knockout proton from a nucleus A and a free nucleon, is [moderately] sensitive to many-body effects such as meson-exchange currents (MEC), isobar currents (IC), and final-state interactions (FSI) [2, 3, 4]. Changes to the measured observables in nuclei due to these many-body effects are possible. It is also hypothesized that the form factors may be modified by the nuclear medium [5], which would also affect this ratio. Distinguishing between the many-body effects and an in-medium modification of the proton's form factors and structure is possible only by comparing the measurements with theoretical calculations.

So far, the only nuclei used for precision measurements of quasielastic polarization transfer were  $^2\text{H}$  [6, 7, 8],  $^4\text{He}$  [9, 10] and  $^{12}\text{C}$  [11]. These data suggest that the double ratio can be characterized by the proton's virtuality, a measure of how far off-shell the proton is, defined (following [7]) as:

$$\nu \equiv (M_A - \sqrt{M_{A-1}^2 + p_{\text{miss}}^2})^2 - p_{\text{miss}}^2 - M_p^2, \quad (2)$$

where  $M_A$  is the mass of the target nucleus,  $M_{A-1}$  is the residual mass, and  $p_{\text{miss}}$  is the missing momentum (determined for each event). Note that this definition of virtuality depends not only on  $p_{\text{miss}}$ , but also on  $E_{\text{miss}}$  (indirectly through  $M_{A-1}$ ).

The measurements of the double ratio for  $^2\text{H}$  and  $^4\text{He}$  (as functions of virtuality) appear in very good agreement with one another in the range where the virtualities overlap. The measurements taken with carbon agrees with the data taken with  $^2\text{H}$  and  $^4\text{He}$  when the virtuality is large; however, when the virtuality is small, the measurements taken for protons knocked out of the  $1p_{3/2}$ -shell of  $^{12}\text{C}$  deviate from the measurements taken with  $^2\text{H}$  and  $^4\text{H}$  (which only contain  $1s$ -shell protons). Since the polarization ratios for knocked-out protons from the  $1s$  shell are consistent despite having very different nuclear medium densities, the data taken so far shows no evidence that the local medium density affects the form factors.

In order to test the universality of the dependence of the double ratio on the virtuality, we propose to perform a similar experiment with a nucleus much heavier than carbon. We propose to use  $^{40}\text{Ca}$  for several reasons. First, the nuclear structure of  $^{40}\text{Ca}$  is has been well-studied, and is very well-described by the shell model, with well-documented separation between nucleon shells. It is also a double-magic nucleus, that is, the number of protons and the number of neutrons (20 of each) is a magic number, filling all of the nucleon states within the shells up to  $1d_{3/2}$ . It is also significantly more massive than carbon, the most massive nucleus for which we have polarization transfer data. The virtuality range that can be covered with this experiment with  $^{40}\text{Ca}$  ranges from around  $-0.15 \text{ GeV}^2$  to  $-0.015 \text{ GeV}^2$ , covering a wider range than what was covered for  $^{12}\text{C}$  [6] in both high and low virtuality, both for positive and negative  $p_{\text{miss}}$ .

Since there is an overlap in the virtuality ranges available for calcium with the data taken with carbon in the  $1s$  and  $1p$  shells near  $-0.12$  and  $-0.07 \text{ GeV}^2$  respectively, we can determine if the polarization transfer ratio is different for a large nucleus in the same shell

and virtuality as it is for a small nucleus.

DWRIA calculations from Carlotta Giusti [12, 13, 14, 15] predict different behaviors of the double ratio curves around  $p_{\text{miss}} = 0$  (corresponding to small  $\nu$ ) when the proton is knocked out of shells with different angular momentum quantum numbers ( $\ell$  and  $j$ ). For calcium, protons knocked out of the  $1d_{3/2}$  and  $1d_{5/2}$  shells (neither of which exist in the nuclei studied thus far) can be distinguished from one another using the missing energy of the reaction, and thus their double-ratios can be compared to one another.

The  $2s$  shell overlaps in virtuality with both the  $1d$  shells, so a comparison between the  $2s$  and  $1d$  shells may also be made.

It is also worth noting that while the polarization component ratios measured for deuterium were consistent with predictions using FSI, the individual components were not consistent with the predictions[6]. Using a calcium target will shed further light on this anomaly. A similar analysis of the data taken with the  $^{12}\text{C}$  target is underway.

## 2 Simulation with MCEEP

In order to determine the amount of beamtime necessary to obtain the required statistics, we used the MCEEP simulation package [16], which was designed to simulate  $(e, e'p)$  scattering with a given set of cuts representing the kinematic acceptance of a detector. The output events are weighted according to their cross-section. When simulating the calcium quasielastic scattering events with MCEEP, we simulated knockout from each of the shells separately.

We adapted measurements taken at Saclay [17], NIKHEF [18, 19] and the University of Tokyo [20] to create models spectral functions for the protons knocked out of  $1s$ ,  $1p$ ,  $1d_{5/2}$ ,  $2s$ , and  $1d_{3/2}$  shells to use in MCEEP. (Due to the large widths of the  $E_{\text{miss}}$  distributions of the  $1p_{3/2}$  and  $1p_{1/2}$  knockout and the large overlap between them, these shells are combined in our model). The results from MCEEP are shown in Section 6.

## 3 Kinematics

We plan to use the spectrometers A and C for the proton and the electron respectively. Spectrometers A and C respectively have momentum acceptances of  $\pm 10.0\%$  and  $\pm 12.5\%$ . Both have vertical angular acceptances of  $\pm 70$  mrad and horizontal acceptances of  $\pm 100$  mrad. We have chosen 3 settings. The first two settings, A and B, focus on positive and negative  $p_{\text{miss}}$  ranges, respectively. The third setting, C, has a  $p_{\text{miss}}$  spectrum centered at 0, and focuses on the  $2s$ -shell knockout. The purpose of setting C is to overlap between settings A and B in the  $2s$ -shell knockout in order to cross-check them with one another for consistency.

Table 1: Proposed central kinematic settings for the  $^{40}\text{Ca}$  polarization transfer measurement.

Variable		setting		
		A	B	C
$E_{\text{beam}}$	(MeV)	600	600	600
$p_e$	(MeV/c)	400	363	435
$\theta_e$	( $^\circ$ )	81.0	65.0	73.0
$p_p$	(MeV/c)	600	630	645
$\theta_p$	( $^\circ$ )	-36.3	-36.4	-41.3
$\omega$	(MeV)	200	237	165
$ \mathbf{q} $	(MeV/c)	667	555	630
$Q^2$	(GeV $^2$ )	0.405	0.251	0.369

## 4 Target

The target will consist of 3 foils of naturally occurring calcium<sup>1</sup>, with the height of  $h = 20$  mm, thickness of  $t = 0.41$  mm, width of  $w = 4$  mm and with densities of  $\rho = 1.54$  g/cm $^3$ . The target foils will be placed one after the other at a distance of about  $d = 1.5$  cm. (This geometry is based on that of the carbon target used in [11]). In order to reduce the path lengths of the ejected protons and thus to minimize their interaction within the target material, minimize their energy losses and increase the resolution of the vertex determination of the reaction, each foil will be rotated around the  $y$  axis by the angle of  $\phi_t = 40^\circ$  in the positive direction, as shown in Fig. 1. Since the incoming electrons hit the foil at an angle rather than straight on, the effective thickness of the foil along the electron's path is  $t \sec \phi_t$ .

## 5 Proposed Analysis

We will use the  $E_{\text{miss}}$  and  $|p_{\text{miss}}|$  to select events from each shell. The cuts on  $E_{\text{miss}}$  and  $|p_{\text{miss}}|$  for each shell are listed in Table 2. Since we cannot differentiate between the  $1p_{3/2}$  and the  $1p_{1/2}$  shells, the  $1p$  selection cuts include both of them.

The ratio  $P_x/P_z$  will be calculated using the azimuthal asymmetry in the FPP and the novel method detailed in [21].

The data will be separated into categories by shell and divided into multiple bins according to their virtuality. The number of bins for each shell will be determined according to the virtuality range available for that shell, and by the statistics in the shell. These bins

---

<sup>1</sup>96.9%  $^{40}\text{Ca}$

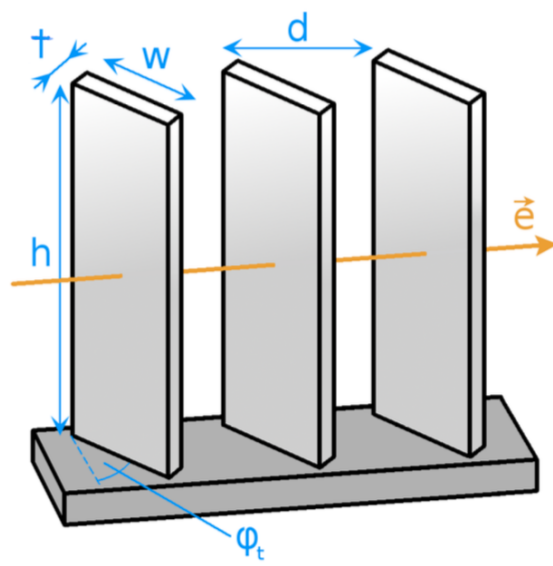


Figure 1: Geometry of the proposed target.

are further divided between the cases where  $p_{\text{miss}}$  is positive and negative.

Shell	$E_{\text{miss}}$ (MeV)		$ p_{\text{miss}} $ (MeV/c)		# of virt. bins
	min	max	min	max	
$1s$	52.0	100.0	0	135	2
$1p$	23.0	37.0	50	–	2
$1d_{5/2}$	13.0	19.0	50	–	2
$2s$	10.2	11.4	0	–	1
$1d_{3/2}$	7.6	9.0	0	–	1

Table 2: Cuts on missing energy and momentum to select each shell. A minimum cut on  $|p_{\text{miss}}|$  is placed on the the  $1p$  and  $1d_{5/2}$  shells in order to reduce contamination from the  $1s$  and  $2s$  shells. Likewise, a maximum cut on  $|p_{\text{miss}}|$  for the  $1s$  shell removes contamination from the  $1p$  shells. The tentative number of bins in virtuality in each shell are also listed.

## 6 Results from MCEEP

Figures 2 through 6 show the missing energy, missing momentum and virtuality spectra for each of the shells simulated in MCEEP, as well as 2-dimensional plot comparing those variables. Figure 7 shows the virtuality spectra after making the shell-selection cuts. Table 3 shows the event rates for each shell at each setting, assuming the beam current is chosen such that the total event rate is 500 Hz.

From Figure 7, we can see that a direct comparison can be made between data taken with a carbon target [11] and the proposed calcium experiment, simultaneously using the same shells, virtualities and  $p_{\text{miss}}$  as one another:

- $1s$ -shell,  $p_{\text{miss}} > 0$ ,  $\nu$  from -0.12 to -0.10 GeV<sup>2</sup>.
- $1s$ -shell,  $p_{\text{miss}} < 0$ ,  $\nu$  from -0.14 to -0.10 GeV<sup>2</sup>.
- $1p$ -shell,  $p_{\text{miss}} < 0$ ,  $\nu$  from -0.08 to -0.05 GeV<sup>2</sup>.

The statistical precision of the measurements of the polarization double ratio in each of these regions are listed in Table 5.

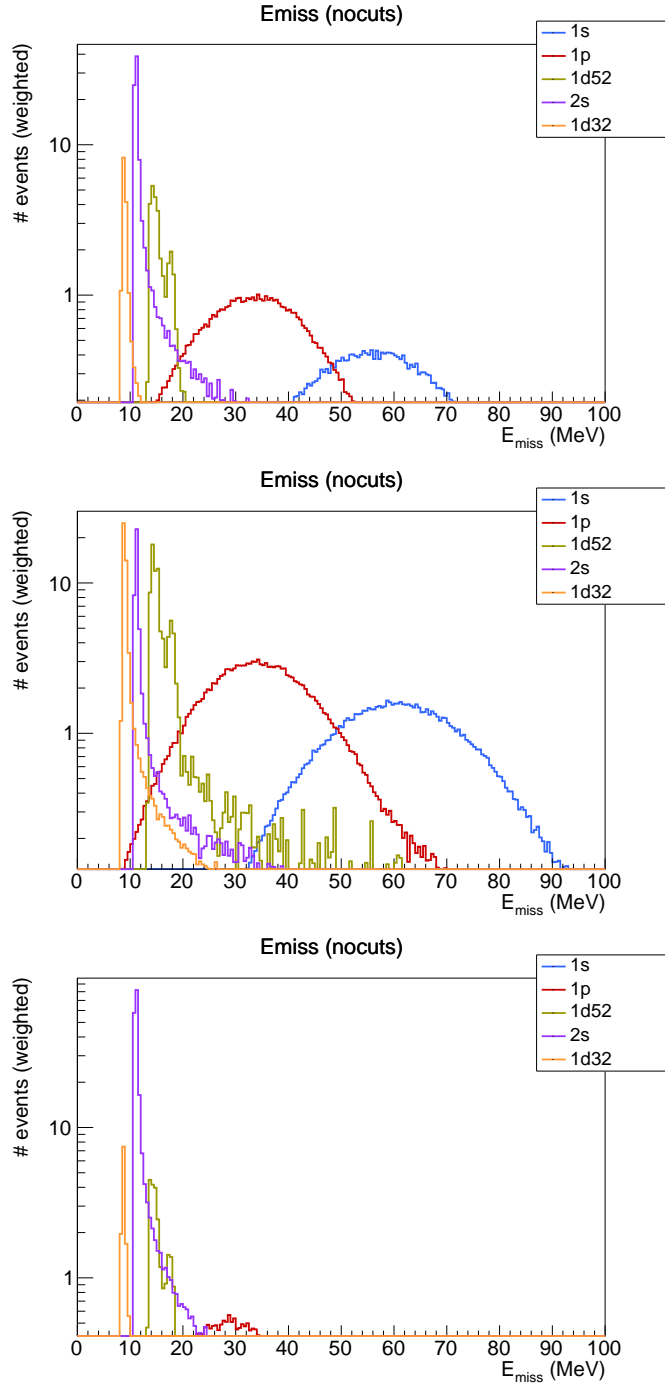


Figure 2: Missing energy spectrum simulated in MCEEP for settings A (top), B (middle) and C (bottom), before making selection cuts on individual shells. The event counts on the  $y$  axis are for an arbitrary runtime, not necessarily the same amount of time as is proposed in this proposal.

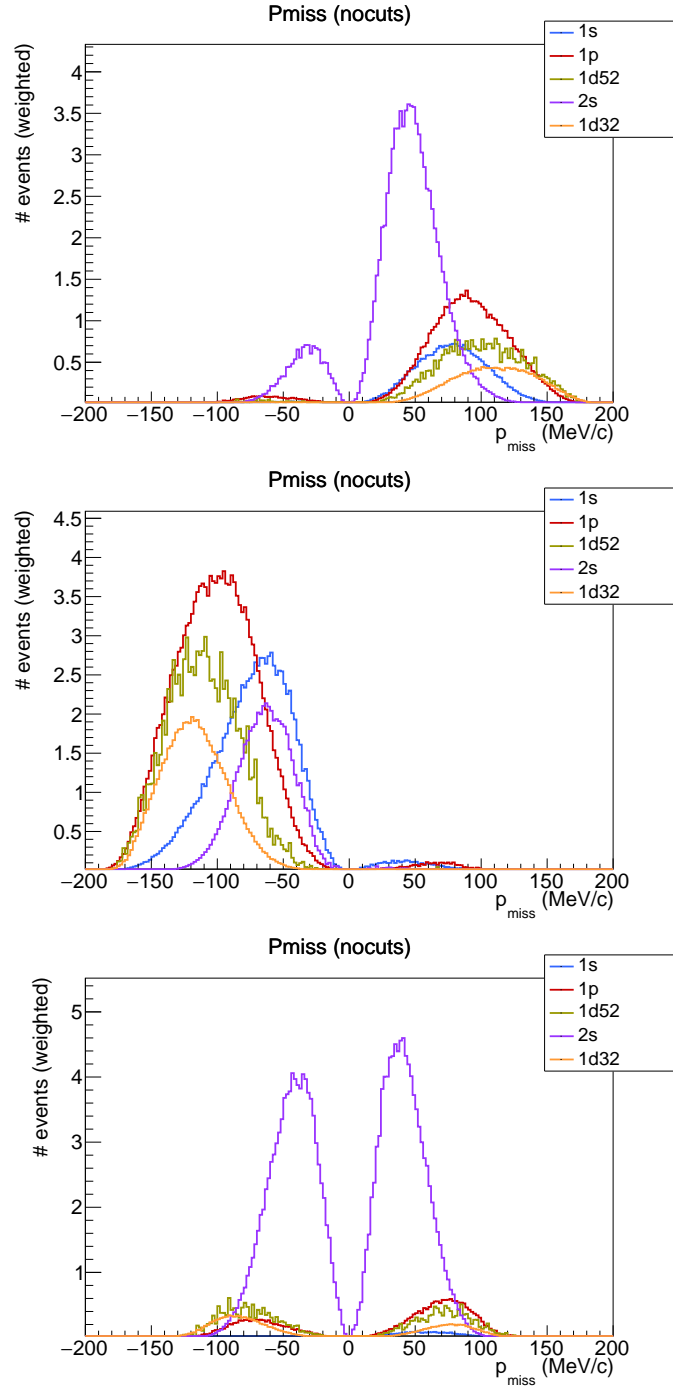


Figure 3: Missing momentum spectrum simulated in MCEEP for settings A (top), B (middle) and C (bottom), before making selection cuts on individual shells.

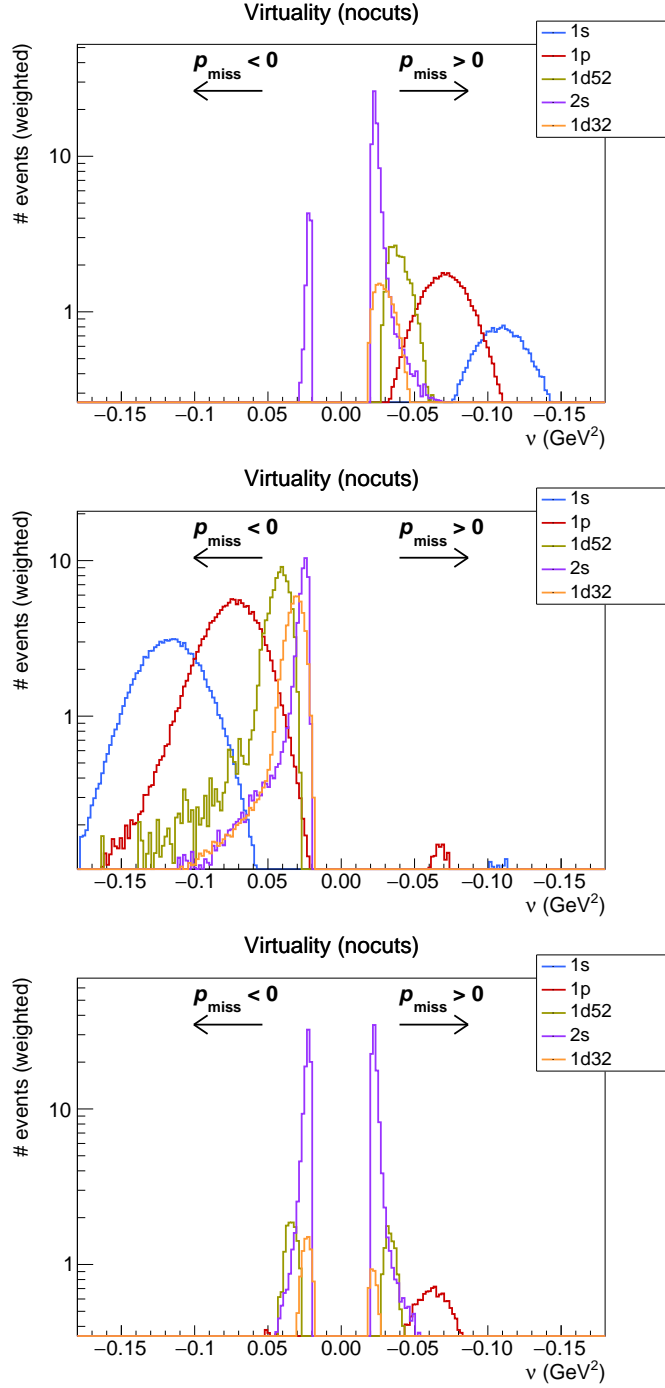


Figure 4: Virtuality spectrum simulated in MCEEP for settings A (top), B (middle) and C (bottom), before making selection cuts on individual shells. Positive (negative)  $p_{\text{miss}}$  is shown on the right (left) side of the graph.

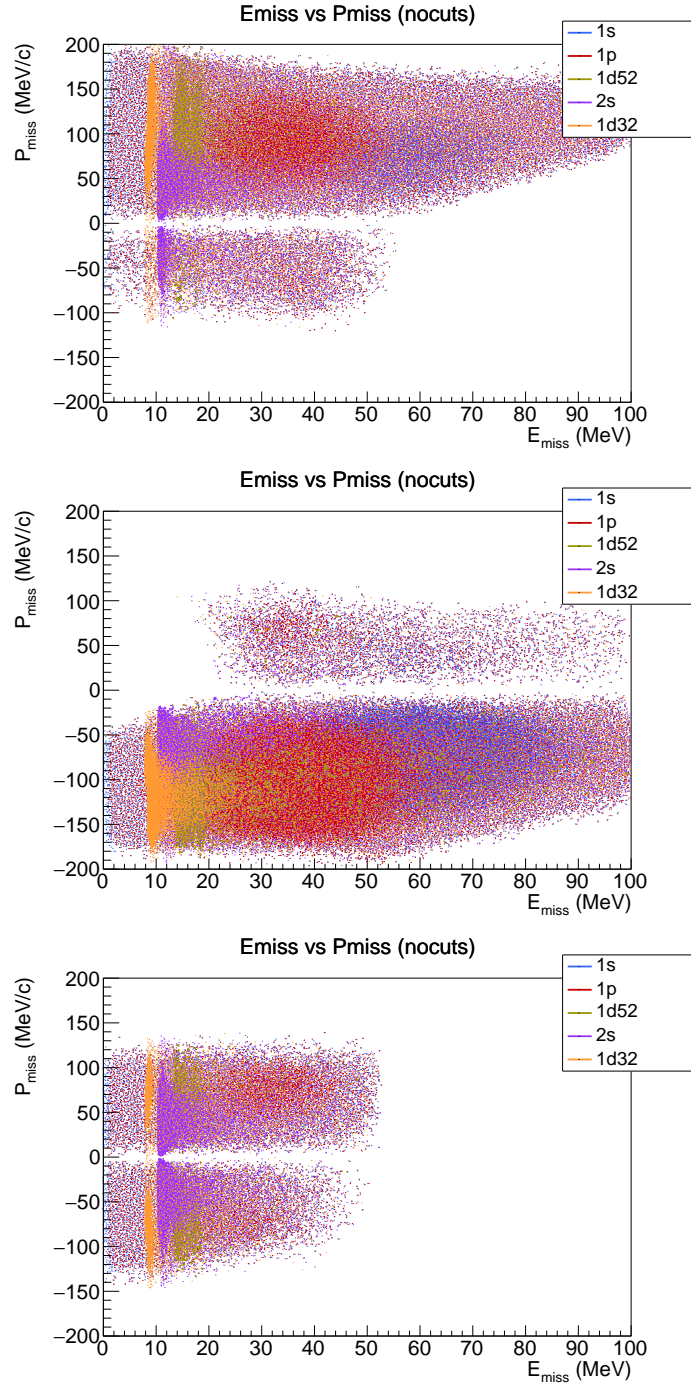


Figure 5:  $E_{\text{miss}}$  vs  $p_{\text{miss}}$  spectrum simulated in MCEEP for settings A (top), B (middle) and C (bottom), before making selection cuts on individual shells.

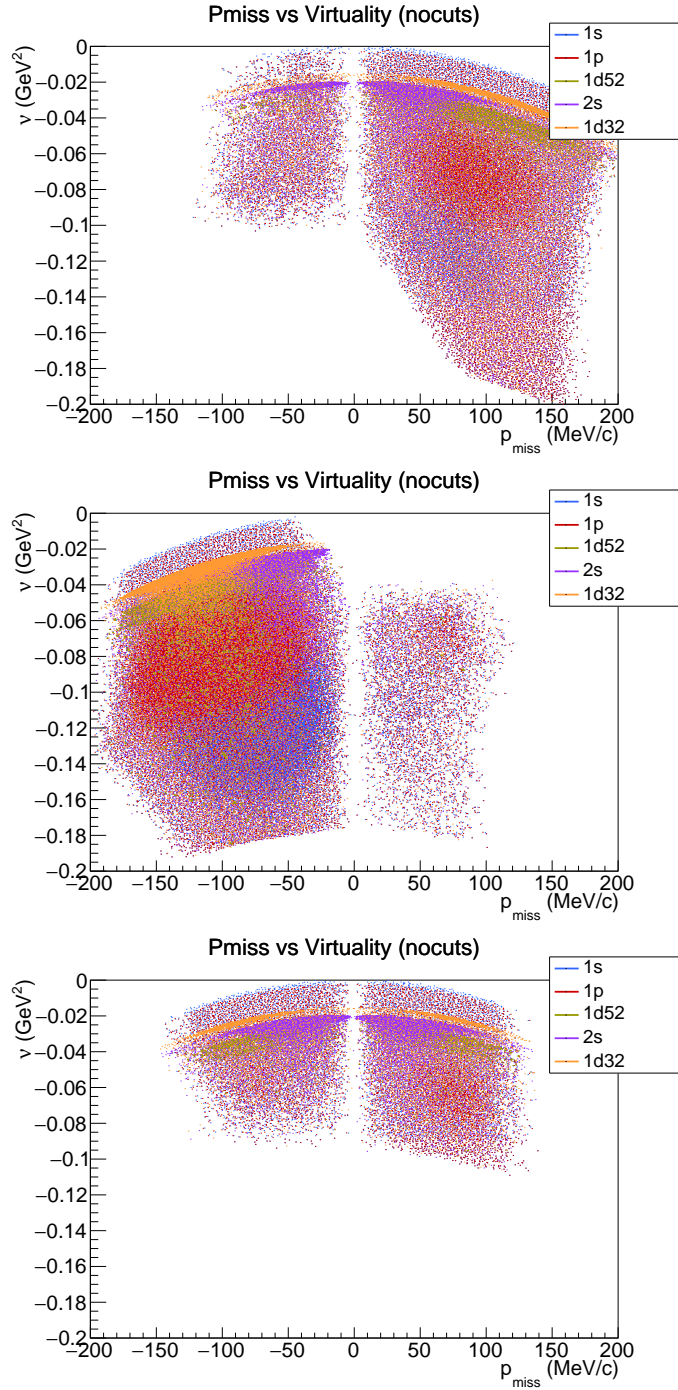


Figure 6:  $p_{\text{miss}}$  vs virtuality spectrum simulated in MCEEP for settings A (top), B (middle) and C (bottom), before making selection cuts on individual shells.

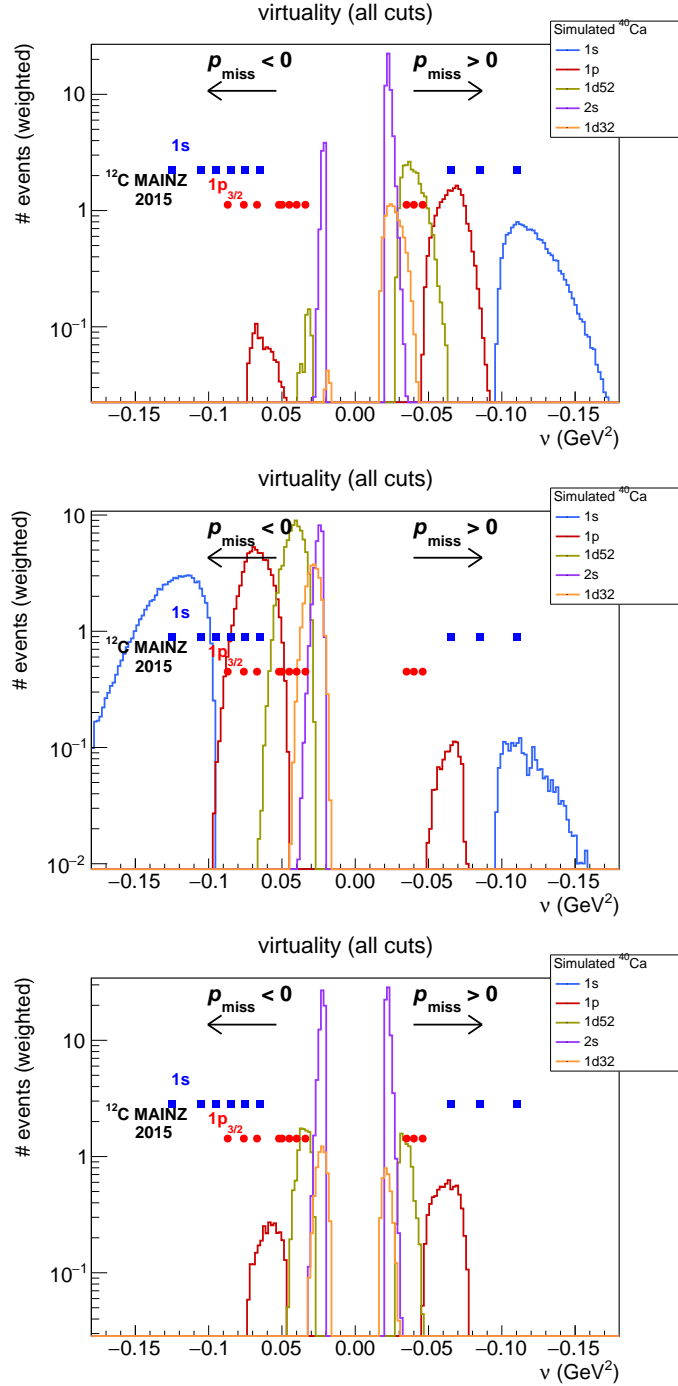


Figure 7: Virtuality spectrum simulated in MCEEP for settings A (top) and B (middle) and C (bottom), after making selection cuts to select individual shells. For comparison, the centers of the bins used in the earlier measurements with carbon [11] are shown as blue squares and red circles.

Setting	Shell	Event Rate (Hz)		Purity (%)
		$p_{\text{miss}} < 0$	$p_{\text{miss}} > 0$	
A	$1s$	0.3	35.8	70.9
	$1p$	3.0	41.2	77.8
	$1d_{5/2}$	1.6	49.9	77.5
	$2s$	26.4	115.1	98.6
	$1d_{3/2}$	0.5	18.6	98.6
B	$1s$	75.9	2.2	77.4
	$1p$	70.4	1.1	82.3
	$1d_{5/2}$	82.6	0.0	84.3
	$2s$	29.9	0.0	90.2
	$1d_{3/2}$	27.3	0.0	98.8
C	$1s$	0.0	0.0	24.1
	$1p$	5.5	14.2	70.7
	$1d_{5/2}$	20.2	15.9	68.2
	$2s$	124.5	126.2	99.4
	$1d_{3/2}$	11.4	6.4	98.3

Table 3: Predicted event rates for kinematic settings A and B, based on simulations in MCEEP. The event rates in the table are scaled so that the total event rate is at the DAQ limit of 500 Hz. The numbers do not add up to 500 because events which cannot be reliably assigned to any of the shells are excluded. These event rates reflect the cross sections and the geometric acceptance and do not take into account detector efficiency nor event quality cuts. The “purity” is the fraction of the events which pass a set of shell-selection cuts where the proton was knocked out of the selected shell.

## 7 Requested Beam-time

Our timeline for the experiment is shown in Table 4. Since the DAQ is limited to 500 Hz, we choose our beam current to bring the DAQ rate as close to 500 Hz. We estimate that  $\approx 20$  hours each day will be spent taking data. The statistical precision listed here are estimated by scaling the statistical errors in [11] by the square root of the ratio of the estimated number of events per bin in [11] to the estimated number of events per bin in the proposed setups, using the numbers of bins per shell in Table 2. Setting C requires significantly less beamtime because it focuses only on the  $2s$  shell, and therefore only has two bins: (positive  $p_{\text{miss}}$  and negative  $p_{\text{miss}}$ , both in a very narrow virtuality range).

Of special interest are the regions where the shell, the direction of  $p_{\text{miss}}$ , and the virtuality overlap between the proposed dataset and the data taken with carbon in [11], since this allows a direct comparison between calcium and carbon. The statistical uncertainties on the overlap regions are listed in Table 5.

Table 4: Timeline for running experiment. Estimated statistical precisions are estimated using the error bars in [11]. The size of the error bars range from shell to shell, depending on the statistics. The listed estimated statistical precisions are for the combinations of shell and  $p_{\text{miss}}$  direction for which sufficient statistics exist, which are listed in the two rightmost columns.

	# of Days	Beam ( $\mu\text{A}$ )	Statistical Precision	Shells		Events (M)	
				$p_{\text{miss}} < 0$	$p_{\text{miss}} > 0$	Raw	Cut
Setup/Test Run	2	—	—	—	—	—	—
Setting A	12	19.7	2.4 to 6.2%	$2s$ only	all shells	432	4.32
Setting B	12	10.4	4.1 to 5.0%	all shells	none	432	4.32
Setting C	4	18.9	4.0%	$2s$ only	$2s$ only	144	1.44

Table 5: Statistical uncertainties of the overlapping regions between our proposed experiment and the existing data with carbon [11]. (See Figure 7.) Numbers of events assume beam is on for 20 hours, and that 1% of raw events pass quality cuts.

$p_{\text{miss}}$	Shell	$\nu$ range ( $\text{GeV}^2$ )	Stat. Precision
+	$1s$	-0.12 to -0.10	6.2%
-	$1s$	-0.14 to -0.10	4.2%
-	$1p$	-0.04 to -0.08	4.4%

## 8 Appendix A: Other Factors Affecting Experimental Sensitivity

In addition to the number of events, the statistical sensitivity of this experiment depends on three other factors: the spin precession inside the spectrometer, the analyzing power of the carbon, and the magnitude of the polarization transfer. The effects of these on the sensitivity can be estimated by comparing to the previously taken datasets in [11], which used the carbon target. The following tests were done to determine if there were any large factors that might severely limit the sensitivity of our experiment.

First, it is essential that the protons precess through the magnetic fields such that the longitudinal component of the polarization at the target ( $P_z^{(\text{target})}$ ) transforms into one of the transverse components at the FPP ( $P_x^{(\text{FPP})}$ ). The magnitude of this component of the precession matrix,  $S_{xz}$ , is then essential to obtaining an accurate measurement of  $P_z^{(\text{target})}$ . We use the program QSPIN [22] to calculate the precession for a given set of kinematics. The value of  $S_{xz}$  depends most strongly on the initial angle in the bend-plane ( $\phi$ ), as this determines the path-length of the proton. With our proposed kinematics, the reference momenta in Spectrometer A are 600-645 MeV, yielding values of  $S_{xz}$  (for  $\phi = 0$ ) of 0.54-0.61. For comparison, the kinematics settings used with carbon in [11] had  $S_{xz} = 0.64$  at  $\phi = 0$ .

The analyzing power of the carbon in the FPP also depends on the proton momentum, increasing in sensitivity with higher proton momentum. The proton momenta in our proposal are comparable to those in [11], so this will not have a large effect on the sensitivity of the experiment.

The third factor to consider is the magnitude of the polarization transfer ( $\sqrt{P_x^2 + P_y^2}$ ). This can be analytically estimated using the polarization transfer on hydrogen for the same kinematics. For the central kinematics of the three proposed settings, the free-proton polarization transfer magnitudes are 0.82, 0.65, and 0.76. In the two settings used in [11], these values were 0.84 and 0.49. However, since we do not know *a priori* how much the polarization transfer magnitude for calcium differs from that of hydrogen, this does not reveal much information about how the sensitivities in the proposed experiment will compare to those in [11].

In summary, we have found that the spin-precession, FPP analyzing power, and the magnitude of the polarization are comparable to those in [11], and do not pose a threat to the sensitivity of our proposed experiment.

## 9 Appendix B: Beam Current

The maximum beam current proposed in this experiment is 19.7  $\mu\text{A}$ , just below the 20  $\mu\text{A}$  limit on the polarized beam available at MAMI [23].

The beam currents used in [11], which were set to  $10 \mu\text{A}$  were limited by the singles rate of Spectrometer A. The proposed beam currents are nearly twice as high as those used in [11], however, our proposed calcium target is slightly less dense and about half as thick as the carbon target was. Hence, the nucleon luminosities ( $\text{barn}^{-1}/\text{s}$  divided by number of nucleons in the target nuclei  $A$ ) in this proposal are slightly smaller than those in the earlier dataset, implying that we will have similar singles rates in the proposed experiment as were obtained in the earlier one. During the test-run, we will be able to confirm if the singles-rate will affect the beam-current that can be used in our experiment, and if necessary to make small adjustments to the beam current.

## References

- [1] A. I. Akhiezer and M. Rekalov, *Sov. J. Part. Nucl.* **4**, 277 (1974), [*Fiz. Elem. Chast. Atom. Yadra*4,662(1973)].
- [2] J.-M. Laget, *Nucl. Phys.* **A579**, 333 (1994).
- [3] J. J. Kelly, *Phys. Rev.* **C59**, 3256 (1999), [nucl-th/9809090](#).
- [4] J. Ryckebusch, D. Debruyne, W. Van Nespen, and S. Janssen, *Phys. Rev.* **C60**, 034604 (1999), [nucl-th/9904011](#).
- [5] R. Schiavilla, O. Benhar, A. Kievsky, L. E. Marcucci, and M. Viviani, *Phys. Rev. Lett.* **94**, 072303 (2005), URL <https://link.aps.org/doi/10.1103/PhysRevLett.94.072303>.
- [6] D. Izraeli et al. (A1), *Phys. Lett.* **B781**, 107 (2018), [1801.01306](#).
- [7] I. Yaron et al. (A1), *Phys. Lett.* **B769**, 21 (2017), [1602.06104](#).
- [8] B. Hu, M. K. Jones, P. E. Ulmer, H. Arenhövel, O. K. Baker, W. Bertozzi, E. J. Brash, J. Calarco, J.-P. Chen, E. Chudakov, et al., *Phys. Rev. C* **73**, 064004 (2006), URL <https://link.aps.org/doi/10.1103/PhysRevC.73.064004>.
- [9] S. Strauch, S. Dieterich, K. A. Aniol, J. R. M. Annand, O. K. Baker, W. Bertozzi, M. Boswell, E. J. Brash, Z. Chai, J.-P. Chen, et al., *Phys. Rev. Lett.* **91**, 052301 (2003), URL <https://link.aps.org/doi/10.1103/PhysRevLett.91.052301>.
- [10] M. Paolone, S. P. Malace, S. Strauch, I. Albayrak, J. Arrington, B. L. Berman, E. J. Brash, B. Briscoe, A. Camsonne, J.-P. Chen, et al. (E03-104 Collaboration), *Phys. Rev. Lett.* **105**, 072001 (2010), URL <https://link.aps.org/doi/10.1103/PhysRevLett.105.072001>.
- [11] D. Izraeli et al. (A1), *Phys. Lett.* **B781**, 95 (2018), [1711.09680](#).

- [12] C. Giusti, *Private communication*.
- [13] E. D. Cooper, S. Hama, B. C. Clark, and R. L. Mercer, Phys. Rev. **C47**, 297 (1993).
- [14] C. Giusti and F. D. Pacati, Nucl. Phys. **A504**, 685 (1989).
- [15] A. Meucci and C. Giusti, Phys. Rev. **C64**, 014604 (2001), [nucl-th/0101034](#).
- [16] P.E. Ulmer, *MCEEP: Monte Carlo for Electro-Nuclear Coincidence Experiments*, [https://hallaweb.jlab.org/software/mceep/mceep\\_v3\\_9.ps](https://hallaweb.jlab.org/software/mceep/mceep_v3_9.ps) (2006), online; accessed 21 October 2018.
- [17] J. Mougey, M. Bernheim, A. Bussiere, A. Gillibert, X. H. Phan, M. Priou, D. Royer, I. Sick, and G. J. Wagner, Nucl. Phys. **A262**, 461 (1976).
- [18] L. Lapikas, Nucl. Phys. **A553**, 297c (1993).
- [19] M. C. Atkinson, H. P. Blok, L. Lapikás, R. J. Charity, and W. H. Dickhoff (2018), 1808.08895.
- [20] K. Nakamura, S. Hiramatsu, T. Kamae, H. Muramatsu, N. Izutsu, and Y. Watase, Nucl. Phys. **A271**, 221 (1976).
- [21] D. Izraeli, I. Mardor, E. O. Cohen, M. Duer, T. Y. Izraeli, I. Korover, J. Lichtenstadt, and E. Piasetzky, JINST **13**, P07029 (2018), 1803.06729.
- [22] T. Pospischil, Ph.D. thesis, Mainz U., Inst. Kernphys. (2000), URL <http://nbn-resolving.de/urn:nbn:de:hebis:77-1113>.
- [23] M. Mihovilovic, *Private communication*.